Research Article | Vol. 28, No. 11 / 25 May 2020 / Optics Express 16772

Optics EXPRESS

Random sources generating hollow array beams

JIA XU, KEMING PAN, AND DAOMU ZHAO*

Zhejiang Province Key Laboratory of Quantum Technology and Device, Department of Physics, Zhejiang University, Hangzhou 310027, China
*zhaodaomu@yahoo.com

Abstract: A novel class of partially coherent light sources that can yield stable optical lattice termed hollow array in the far field is introduced. The array dimension, the distance of hollow lobes intensity profile, the size and shape of the inner and outer lobe contours and other features can be flexibly controlled by altering the source parameters. Further, every lobe can be shaped with polar and Cartesian symmetry and even combined to form nested structures. The applications of the work are envisioned in material surface processing and particle trapping.

1. Introduction

It is well known in statistical optics that the intensity distribution of in the far field is closely related to the structure of the correlation function of a field in the source plane [1]. Since Gori and Santarsiero demonstrated mathematical description of devising genuine special correlation functions, generation of wide-sense stationary fields with prescribed far-field statistical properties has been the area of active research [2]. Some important progresses have been made in recent years. A series of far fields with prescribed spectral density are capable to be produced by source models which can be proved by simulation and experiment [3–11].

Light fields of spatial periodic structure are of particular interest for photonic lithography [12,13], microfluidic sorting [14], trapping and cooling ultracold atoms [15,16]. Various light beams of spatially periodic arrays have been reported in theoretical predicting and experimental techniques [17–23]. Meanwhile, with the wide application of hollow beams in focusing [24], guiding particles [25], optical communications [26] and trapping atoms [27]. The models of hollow beams have received much attention and been studied extensively, including hollow Gaussian beams [28,29], controllable dark-hollow beams (CDHBs) [30], hypergeometric-Gaussian beams [31,32], hollow sinh-Gaussian beams [33–35], higher-order Bessel beams [36], and Laguerre–Gaussian beams [37]. Then, a number of experimental techniques for generating hollow beams have been reported, such as phase plate [38], hollow optical fibers [39], spatial filtering [40], optical holography [41].

In this work, we introduce a model for correlation function of a planar source, which uses the Fourier transform of the multi-Gaussian array family of functions and sets legitimate difference operations. Such a source with arbitrary intensity distribution can naturally evolve into a periodic array profile consisting of fully controllable individual hollow lobes when propagating. Moreover, it is interesting that every lobe can be shaped with polar and Cartesian symmetry and even combine both two to form nested structures. The most important feature of the array in this article is that it remains structurally invariant on further propagation when the pattern is formed in the far field. Further, not only can the array lobes adjust symmetry effectively, but also they can control the size and shape of the inner and outer contours separately. Therefore, the hollow array beams can be acted as the versatile potential field to trap particles.

2. Model for the the hollow multi-Gaussian Schell-model array source

Suppose that a random beam-like field is generated by a planar source located in the plane $z = 0$ and propagates along the positive z direction. The cross-spectral density (CSD) of the field at the

#395226 https://doi.org/10.1364/OE.395226
Journal © 2020 Received 15 Apr 2020; revised 10 May 2020; accepted 13 May 2020; published 19 May 2020

Optics EXPRESS

source plane is defined by a two-point correlation function [1]:

$$W^{(0)}(\boldsymbol{\rho}_1, \boldsymbol{\rho}_2; \omega) = \langle E^*(\boldsymbol{\rho}_1; \omega) E(\boldsymbol{\rho}_2; \omega) \rangle, \tag{1}$$

where E denotes the field fluctuating in the source plane, and the angular brackets signify its ensemble average. The asterisk denotes the complex conjugate. For brevity, in what follows the angular frequency dependence of all quantities of interest will be omitted but implied. And the general form for any Schell-model CSD function of a random field at the planar source surface is [2]

$$W^{(0)}(\boldsymbol{\rho}_1, \boldsymbol{\rho}_2) = \sqrt{S(\boldsymbol{\rho}_1)}\sqrt{S(\boldsymbol{\rho}_2)}\mu(\boldsymbol{\rho}_2 - \boldsymbol{\rho}_1), \tag{2}$$

where $S(\boldsymbol{\rho})$ is the spectral density at a source point with position vector $\boldsymbol{\rho}$, and $\mu(\boldsymbol{\rho}_2 - \boldsymbol{\rho}_1)$ is the spectral degree of coherence at a pair of points in the source plane with position vectors $\boldsymbol{\rho}_1$ and $\boldsymbol{\rho}_2$. To be a mathematically genuine correlation function, the cross-spectral density must correspond to a non-negative definite kernel, which is fulfilled if the CSD function can be written as a superposition intergral of the form [2]

$$W^{(0)}(\boldsymbol{\rho}_1, \boldsymbol{\rho}_2) = \int p(\mathbf{v}) H_0^*(\boldsymbol{\rho}_1, \mathbf{v}) H_0(\boldsymbol{\rho}_2, \mathbf{v}) d^2v, \tag{3}$$

where $p(\mathbf{v})$ is an arbitrary non-negation weight function which governs the profile of the correlation function, and $H_0(\boldsymbol{\rho}, \mathbf{v})$ is an arbitrary kernel which governs the correlation class of a light field. For Schell-model sources, $H_0(\boldsymbol{\rho}, \mathbf{v})$ has a Fourier-like form, i.e.

$$H_0(\boldsymbol{\rho}, \mathbf{v}) = \tau(\boldsymbol{\rho}) \exp(-2\pi i \mathbf{v} \cdot \boldsymbol{\rho}), \tag{4}$$

where $\tau(\boldsymbol{\rho})$ is an amplitude profile function. Then, substitution from Eq. (4) into Eq. (3) leads to the expression

$$W^{(0)}(\boldsymbol{\rho}_1, \boldsymbol{\rho}_2) = \tau^*(\boldsymbol{\rho_1})\tau(\boldsymbol{\rho_2})\mu(\boldsymbol{\rho}_2 - \boldsymbol{\rho}_1), \tag{5}$$

where

$$\mu(\boldsymbol{\rho}_2 - \boldsymbol{\rho}_1) = \int p(\mathbf{v}) \exp[-2\pi i \mathbf{v} \cdot (\boldsymbol{\rho}_2 - \boldsymbol{\rho}_1)] d^2v. \tag{6}$$

The choice of $\mu(\boldsymbol{\rho}_2 - \boldsymbol{\rho}_1)$ defines a family of source with different weight function $p(\mathbf{v})$. And let us set the amplitude profile for function $\tau(\boldsymbol{\rho})$ with the rms source width σ_0, i.e.

$$\tau(\boldsymbol{\rho}) = \exp\left[-\rho^2/\left(4\sigma_0^2\right)\right]. \tag{7}$$

To generate a far-field with flat-top beams, let us now choose the spectral degree of coherence to be

$$\mu(\boldsymbol{\rho}_2 - \boldsymbol{\rho}_1) = \frac{1}{C_0} \sum_{l=1}^{L} \frac{(-1)^{l-1}}{l} \begin{pmatrix} L \\ l \end{pmatrix} \exp\left[-\frac{(x_2 - x_1)^2}{2l\delta_x^2} - \frac{(y_2 - y_1)^2}{2l\delta_y^2}\right], \tag{8}$$

where $C_0 = \sum_{l=1}^{L} \frac{(-1)^{l-1}}{l} \begin{pmatrix} L \\ l \end{pmatrix}$ is the normalization factor, $\begin{pmatrix} L \\ l \end{pmatrix}$ are binomial coefficients, δ_x and δ_y are the effective correlation widths. Now let us add array term to produce $N \times M$ optical coherence lattice. In this case, we introduce a novel class of the degree of potential correlation

$$\begin{aligned} \mu_c(\boldsymbol{\rho}_2 - \boldsymbol{\rho}_1) = & \frac{1}{C_0 NM} \sum_{l=1}^{L} \frac{(-1)^{l-1}}{l} \begin{pmatrix} L \\ l \end{pmatrix} \exp\left[-\frac{(x_2 - x_1)^2}{2l\delta_x^2} - \frac{(y_2 - y_1)^2}{2l\delta_y^2}\right] \\ & \times \sum_{n=-P}^{P} \cos\left[\frac{2\pi n R_x (x_2 - x_1)}{\delta_x}\right] \sum_{m=-Q}^{Q} \cos\left[\frac{2\pi m R_y (y_2 - y_1)}{\delta_y}\right], \end{aligned} \tag{9}$$

where R_x and R_y are coherence parameters. $\cos(x)$ is the cosine function, $P = (N-1)/2$ and $Q = (M-1)/2$. Then in order to generate a far-field with $N \times M$ hollow multi-Gaussian array

Optics EXPRESS

beams, now one can choose two different spectral degree of coherence in Eq. (9) to make a difference, and arrive at

$$\mu_C(\boldsymbol{\rho}_2-\boldsymbol{\rho}_1)=\mu_{c1}(\boldsymbol{\rho}_2-\boldsymbol{\rho}_1)-\mu_{c2}(\boldsymbol{\rho}_2-\boldsymbol{\rho}_1), \tag{10}$$

where

$$\mu_{ct}(\boldsymbol{\rho}_2-\boldsymbol{\rho}_1)=\frac{1}{C_{0t}NM}\sum_{l=1}^{L_t}\frac{(-1)^{l-1}}{l}\begin{pmatrix}L_t\\ l\end{pmatrix}\exp\left[-\frac{(x_2-x_1)^2}{2l\delta_{tx}^2}-\frac{(y_2-y_1)^2}{2l\delta_{ty}^2}\right]\quad(t=1,2). \tag{11}$$
$$\times\sum_{n=-P}^{P}\cos\left[\frac{2\pi nR_{tx}(x_2-x_1)}{\delta_{tx}}\right]\sum_{m=-Q}^{Q}\cos\left[\frac{2\pi mR_{ty}(y_2-y_1)}{\delta_{ty}}\right]$$

On taking the Fourier-transform of $\mu_c(\boldsymbol{\rho}_2-\boldsymbol{\rho}_1)$ we obtain the formula for the weight function:

$$p_c(\mathbf{v})=p_1(\mathbf{v})-p_2(\mathbf{v}), \tag{12}$$

where

$$p_t(\mathbf{v})=\frac{\delta_{tx}^2\delta_{ty}^2}{C_{0t}NM}\sum_{l=1}^{L_t}\frac{(-1)^{l-1}}{l}\begin{pmatrix}L_t\\ l\end{pmatrix}\exp\left(-\frac{l\delta_{tx}^2v_x^2}{2}-\frac{l\delta_{ty}^2v_y^2}{2}\right)$$
$$\times\sum_{n=-P}^{P}\cosh\left(2l\delta_{tx}\pi nR_{tx}v_x\right)\exp\left(-2l\pi^2n^2R_{tx}^2\right)\qquad(t=1,2), \tag{13}$$
$$\times\sum_{m=-Q}^{Q}\cosh\left(2l\delta_{ty}\pi mR_{ty}v_y\right)\exp\left(-2l\pi^2m^2R_{ty}^2\right)$$

and $\cosh(x)$ is the hyperbolic cosine function. Figure 1 shows the behavior of the degree of potential correlation given by Eq. (10) as a function of $x_d=x_2-x_1$ and $y_d=y_2-y_1$. Obviously, function $p(\mathbf{v})$ represents a family of hollow flat-top array profiles.

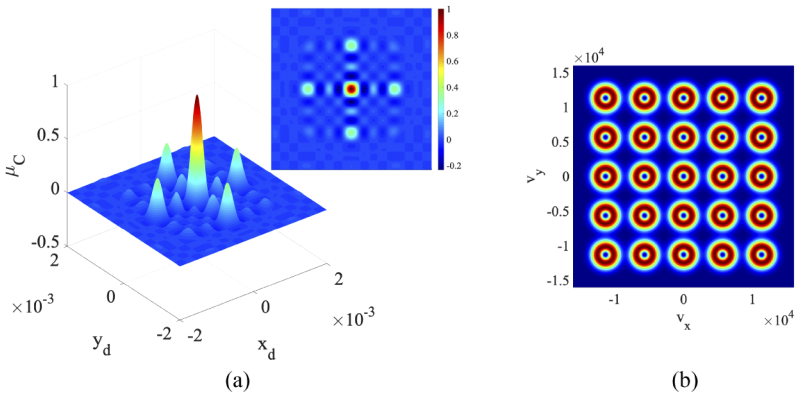

Fig. 1. Illustration of the degree of coherence (a) for a the hollow multi-Gaussian Schell-model array source calculated from Eq. (10) and function $p(\mathbf{v})$ (b) calculated from Eq. (12). Calculated parameters are set as follows: $M=5, N=5, L_1=2, L_2=1, \delta=1mm, R=0.9m,$ $\lambda=632.8nm$.

For function $p(\mathbf{v})$ to be non-negative, based on $p_1(\mathbf{v})\geqslant 0$ and $p_2(\mathbf{v})\geqslant 0$ for any values of 2D vector $\mathbf{v}$, we must set parameter $L_1>L_2$.

Optics EXPRESS

Then, on substituting from Eqs. (10) and (7) into Eq. (5), we obtain the CSD function of the form

$$W^{(0)}(\boldsymbol{\rho}_1, \boldsymbol{\rho}_2) = \exp\left(-\frac{\rho_1^2 + \rho_2^2}{4\sigma_0^2}\right)\left[\mu_{c1}(\boldsymbol{\rho}_2 - \boldsymbol{\rho}_1) - \mu_{c2}(\boldsymbol{\rho}_2 - \boldsymbol{\rho}_1)\right]. \tag{14}$$

We will term such a source the hollow multi-Gaussian Schell-model array (HGSMA) source.

In the following, the CSD function of the radiated field in the far zone at two points specified by position vectors $\mathbf{r}_1 = r_1\mathbf{s}_1$ and $\mathbf{r}_2 = r_2\mathbf{s}_2$, with $\mathbf{s}_1^2 = \mathbf{s}_2^2 = 1$. And the field in the far zone of the source is given by the expression

$$W^{(\infty)}(r_1\mathbf{s}_1, r_2\mathbf{s}_2) = (2\pi k)^2 \cos\theta_1 \cos\theta_2 \tilde{W}^{(0)}(-k\mathbf{s}_{1\perp}, -k\mathbf{s}_{2\perp}) \exp\left[ik(\mathbf{r}_2 - \mathbf{r}_1)\right]/(r_1 r_2), \tag{15}$$

where $k = 2\pi/\lambda$ is the wave number of the field, λ being the wavelength, $\mathbf{s}_\perp$ is the projection of $\mathbf{s}$ onto the source plane, $\mathbf{s}_\perp = \sin\theta$, $\mathbf{s}_z = \cos\theta$, and

$$\tilde{W}^{(0)}(\mathbf{f}_1, \mathbf{f}_2) = (2\pi)^{-4} \iint W^{(0)}(\boldsymbol{\rho}_1, \boldsymbol{\rho}_2) \exp\left[-i(\mathbf{f}_1 \cdot \boldsymbol{\rho}_1 + \mathbf{f}_2 \cdot \boldsymbol{\rho}_2)\right] d^2\rho_1 d^2\rho_2 \tag{16}$$

is the four-dimensional Fourier transform.

On substituting Eq. (14) first into Eq. (16) and then into Eq. (15), we obtain the following expression for the CSD in the far field:

$$W_C^{(\infty)}(r_1\mathbf{s}_1, r_2\mathbf{s}_2) = W_1^{(\infty)}(r_1\mathbf{s}_1, r_2\mathbf{s}_2) - W_2^{(\infty)}(r_1\mathbf{s}_1, r_2\mathbf{s}_2), \tag{17}$$

where

$$\begin{aligned} W_t^{(\infty)}(r_1\mathbf{s}_1, r_2\mathbf{s}_2) = & \frac{k^2\sigma_0^2 \cos\theta_1 \cos\theta_2 \exp\left[ik(r_2 - r_1)\right]}{2C_{0t}NMr_1r_2} \sum_{l=1}^{L_t} \frac{(-1)^{l-1}}{l} \begin{pmatrix} L_t \\ l \end{pmatrix} \\ & \times \frac{1}{\sqrt{a_{tx}a_{ty}}} \exp(b_{tx}) \exp(b_{ty}) \\ & \times \sum_{n=-P}^{P} \cosh\left[\frac{nc_{tx}k}{2a_{tx}}(s_{1x} + s_{2x})\right] \exp\left(-\frac{n^2c_{tx}^2}{a_{tx}}\right) \\ & \times \sum_{m=-Q}^{Q} \cosh\left[\frac{mc_{ty}k}{2a_{ty}}(s_{1y} + s_{2y})\right] \exp\left(-\frac{m^2c_{ty}^2}{a_{ty}}\right) \end{aligned} \qquad (t = 1, 2), \tag{18}$$

and

$$\begin{aligned} a_{tj} &= \frac{1}{8\sigma_0^2} + \frac{1}{2l_t\delta_{tj}^2}, \\ b_{tj} &= \frac{-k^2}{2}\left[\sigma_0^2(s_{2j} - s_{1j})^2 + \frac{(s_{2j} + s_{1j})^2}{8a_{tj}}\right], \quad (j = x, y; t = 1, 2). \\ c_{tj} &= \frac{\pi R_{tj}}{\delta_{tj}}, \end{aligned} \tag{19}$$

It follows from Eq. (17), with the formula $\mathbf{r}_1 = \mathbf{r}_2 = \mathbf{r}$, that the far-field spectral density distribution takes the form

$$S_C^{(\infty)}(r\mathbf{s}) = S_1^{(\infty)}(r\mathbf{s}) - S_2^{(\infty)}(r\mathbf{s}), \tag{20}$$

Optics EXPRESS

where

$$S_t^{(\infty)}(r\mathbf{s}) = \frac{k^2\sigma_0^2\cos^2\theta}{2C_{0t}NMr^2}\sum_{l=1}^{L_t}\frac{(-1)^{l-1}}{l}\begin{pmatrix} L_t \\ l \end{pmatrix} \times \frac{1}{\sqrt{a_{tx}a_{ty}}}\exp\left(-\frac{k^2s_x^2}{4a_{tx}}\right)\exp\left(-\frac{k^2s_y^2}{4a_{ty}}\right) \times \sum_{n=-P}^{P}\cosh\left(\frac{nc_{tx}}{a_{tx}}ks_x\right)\exp\left(-\frac{n^2c_{tx}^2}{a_{tx}}\right) \times \sum_{m=-Q}^{Q}\cosh\left(\frac{mc_{ty}}{a_{ty}}ks_y\right)\exp\left(-\frac{m^2c_{ty}^2}{a_{ty}}\right) \quad (t=1,2), \tag{21}$$

In order for the function $W^{(0)}(\boldsymbol{\rho}_1, \boldsymbol{\rho}_2)$ to generate a beam, the far-field spectral density in Eq. (20) must be negligible except for directions within a narrow solid angle about the z axis. This is so if

$$\exp\left(-\frac{k^2s_j^2}{4a_{tj}}\right) \approx 0, \quad j = x, y; t = 1, 2. \tag{22}$$

Thus, the necessary and sufficient conditions for the source Eq. (12) to generate a beam are

$$\frac{1}{4\sigma_0^2} + \frac{1}{\delta_{tj}^2} \ll \frac{2\pi^2}{\lambda^2}, \quad j = x, y; t = 1, 2. \tag{23}$$

In the following, let us investigate influences of structural parameters on distribution of normalized spectral intensity of far field.

In Fig. 2, the spectral intensity produced by the weight function is given by Eq. (12) are plotted. It can be clearly seen that the far field indeed displays a HGSMA distribution. Besides, from the Figs. 2(a) and 2(b), the HGSMA pattern presents identical and equivalent interval hollow profile lobes. Moreover, M controls the number of rows, and N controls the number of columns. Furthermore, as shown in Figs. 2(b) and 2(c), it is simple to control the radial distance of each lobe with the parameter R. With the increasing of the value of parameter R, the radial distance of the array will also increase. When setting $R_x = R_y$, the intensity distribution of the far field must be symmetric. But the distance of lobes can be unequal with different dimensions by assigning different value along x and y directions, and the corresponding result is displayed in Fig. 2(d).

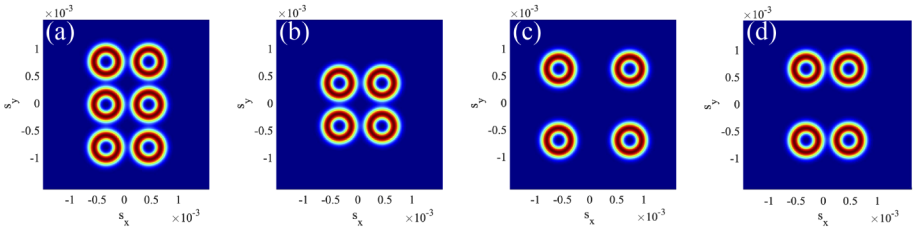

Fig. 2. Influence of parameter M, N and R on distribution of normalized spectral intensity of far field: $L_1 = 2$, $L_2 = 1$, $\delta = 1mm$, $\sigma_0 = 1mm$; (a) $M = 3$, $N = 2$, $R_x = R_y = 1.2m$; (b) $M = 2$, $N = 2$, $R_x = R_y = 1.2m$; (c) $M = 2$, $N = 2$, $R_x = R_y = 2m$; (d) $M = 2$, $N = 2$, $R_x = 1.2m$, $R_y = 2m$.

Figure 3 reveals the influence of parameters L and the effective correlation length δ on distributions of normalized spectral intensity. Comparing with these three figures in Figs. 3(a)-(c),

Optics EXPRESS

one may find that, with parameter L_1 is unchanged and L_2 increasing, the hollow area in the central region continuously increases. In other words, the larger the difference between L_1 and L_2, the larger the hollow area in the center. Besides, each lobe profile is isotropic with the same effective correlation length along the x and y directions. Moreover, when choosing the diffident effective correlation length along the x and y directions, each lobe profile is anisotropic. It can be clearly seen from Figs. 3(c) and 3(d) that when δy is smaller than δx, the long axis is in the y direction, on the contrary, when δy is larger than δx, the long axis is in the x direction.

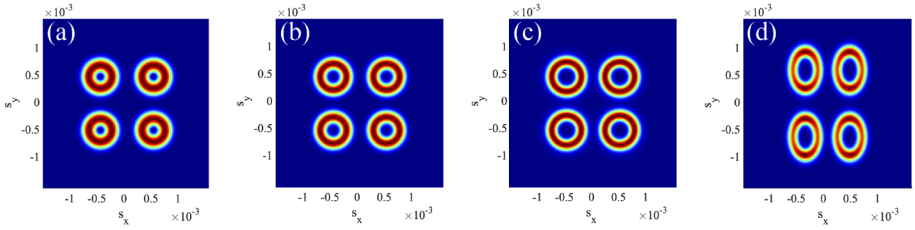

Fig. 3. Influence of parameter L and δ on distribution of normalized spectral intensity of far field: $M = 2, N = 2, R_x = R_y = 1.5m, \sigma_0 = 1mm$; (a) $L_1 = 40, L_2 = 1, \delta_x = \delta_y = 1mm$; (b) $L_1 = 40, L_2 = 5, \delta_x = \delta_y = 1mm$; (c) $L_1 = 40, L_2 = 20, \delta_x = \delta_y = 1mm$; (d) $L_1 = 40, L_2 = 20, \delta_x = 1.2mm, \delta_y = 0.8mm$.

3. Design array lobes with Cartesian symmetry

In the above, the spectral intensity distribution of the far field corresponding to Eq. (10) has a shape of circular hollow array. Furthermore, let us consider an extension which can obtain hollow intensity profiles of every lobe with Cartesian symmetry. In this case, we may choose μ_R in the form

$$\mu_R(\boldsymbol{\rho}_2 - \boldsymbol{\rho}_1) = \mu_{r1}(\boldsymbol{\rho}_2 - \boldsymbol{\rho}_1) - \mu_{r2}(\boldsymbol{\rho}_2 - \boldsymbol{\rho}_1), \tag{24}$$

where

$$\begin{aligned}\mu_{rt}(\boldsymbol{\rho}_2 - \boldsymbol{\rho}_1) = {} & \frac{1}{C_{0t}NM}\sum_{l=1}^{L_t}\frac{(-1)^{l-1}}{\sqrt{l}}\begin{pmatrix} L_t \\ l \end{pmatrix}\exp\left[-\frac{(x_2-x_1)^2}{2l\delta_{tx}^2}\right] \\ & \times\sum_{l=1}^{L_t}\frac{(-1)^{l-1}}{\sqrt{l}}\begin{pmatrix} L_t \\ l \end{pmatrix}\exp\left[-\frac{(y_2-y_1)^2}{2l\delta_{ty}^2}\right] \qquad (t=1,2), \\ & \times\sum_{n=-P}^{P}\cos\left[\frac{2\pi nR_{tx}(x_2-x_1)}{\delta_{tx}}\right]\sum_{m=-Q}^{Q}\cos\left[\frac{2\pi mR_{ty}(y_2-y_1)}{\delta_{ty}}\right]\end{aligned} \tag{25}$$

Figure 4 displays the degree of coherence μ_R and the corresponding distribution for $p(\mathbf{v})$ for the lobes with Cartesian symmetry. Similarly to the circular case, function $p(\mathbf{v})$ represents a family of rectangular hollow array profiles.

Then, on substituting from Eqs. (24) and (7) into Eq. (5), we obtain the CSD function. After combining with Eqs. (15) and (16), with the formula $\mathbf{r}_1 = \mathbf{r}_2 = \mathbf{r}$, the rectangular far-field spectral density distribution takes the form

$$S_R^{(\infty)}(r\mathbf{s}) = S_{r1}^{(\infty)}(r\mathbf{s}) - S_{r2}^{(\infty)}(r\mathbf{s}), \tag{26}$$

Optics EXPRESS

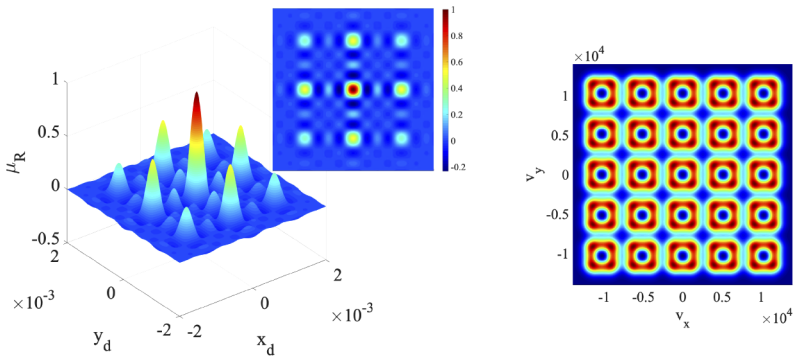

Fig. 4. Illustration of the degree of coherence (a) and its Fourier transform $p(\mathbf{v})$ (b) for the rectangular Hollow multi-Gaussian Schell-model array source corresponding to Eq. (24). Calculated parameters are set as follows: $M = 5$, $N = 5$, $L_1 = 3$, $L_2 = 2$, $\delta = 1mm$, $R = 0.82m$.

$$
\begin{aligned}
S_{rt}^{(\infty)}(r\mathbf{s}) = & \frac{k^2\sigma_0^2\cos^2\theta}{2C_{0t}NMr^2}\sum_{l=1}^{L_t}\frac{(-1)^{l-1}}{\sqrt{l}}\begin{pmatrix} L_t \\ l \end{pmatrix}\frac{1}{\sqrt{a_{tx}}}\exp\left(-\frac{k^2 s_x^2}{4a_{tx}}\right) \\
& \times\sum_{l=1}^{L_t}\frac{(-1)^{l-1}}{\sqrt{l}}\begin{pmatrix} L_t \\ l \end{pmatrix}\frac{1}{\sqrt{a_{ty}}}\exp\left(-\frac{k^2 s_y^2}{4a_{ty}}\right) \\
& \times\sum_{n=-P}^{P}\cosh\left(\frac{nc_{tx}}{a_{tx}}ks_x\right)\exp\left(-\frac{n^2c_{tx}^2}{a_{tx}}\right) \\
& \times\sum_{m=-Q}^{Q}\cosh\left(\frac{mc_{ty}}{a_{ty}}ks_y\right)\exp\left(-\frac{m^2c_{ty}^2}{a_{ty}}\right)
\end{aligned}
\qquad (t = 1, 2). \qquad (27)
$$

Obviously, as the same feather like circular case, Figs. 5(a) and 5(b) present that the parameters M and N are capable of having adjustable number of lobes in row and column, respectively. Furthermore, as shown in Figs. 5(b)-(d), The parameters R_x and R_y can fully control the distance of lobes along the x and y directions. As displayed in Fig. 6(a), it is worth noting that the central hollow intensity distribution of lobes can also reduce to circular distribution with $L_2 = 1$. With the increase of L_2, the size of the central hollow of lobes becomes square and bigger, the corresponding result is displayed in Figs. 6(a)-(c). Comparing with Figs. 6(c) and 6(d), it is clear from the plots that assigning different correlations along the x and y directions it is possible to achieve practically any anisotropic features of the rectangular lobes in the hollow array distribution.

Optics EXPRESS

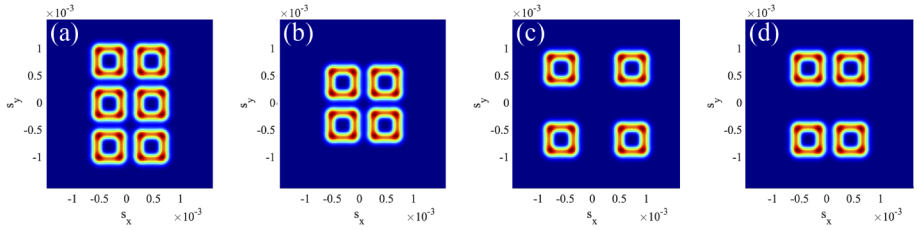

Fig. 5. Influence of parameter M, N and R on distribution of normalized spectral intensity of far field corresponding to Eq. (26): $L_1 = 10$, $L_2 = 8$ and rest parameters as in Fig. 2.

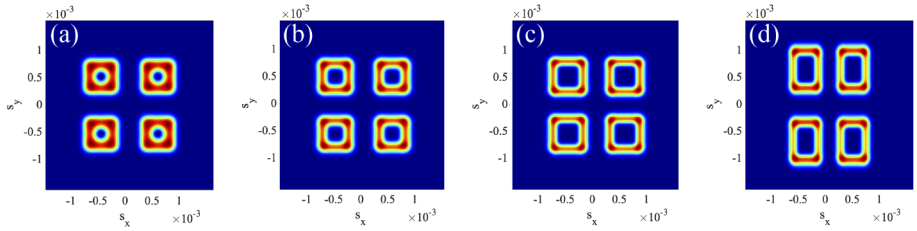

Fig. 6. Influence of parameter L and δ on distribution of normalized spectral intensity of far field corresponding to Eq. (26): (a) $L_1 = 20$, $L_2 = 1$; (b) $L_1 = 20$, $L_2 = 4$; (c) $L_1 = 20$, $L_2 = 18$; (d) $L_1 = 20$, $L_2 = 18$ and the paramenter δ as in Fig. 3.

4. Design a new profile of array lobes

In what follows, linear superposition of the degrees of coherence introduced in Eq. (11) and Eq. (25) may lead to a new optical field with combinations of the individual distribution. In particular, the addition of the degrees of coherence with different weight coefficients leads to radiation of different distributions with desired intensities, i.e.

$$\mu_{CR}(\boldsymbol{\rho}_2 - \boldsymbol{\rho}_1) = a\mu_{c1}(\boldsymbol{\rho}_2 - \boldsymbol{\rho}_1) + b\mu_{r2}(\boldsymbol{\rho}_2 - \boldsymbol{\rho}_1), \tag{28}$$

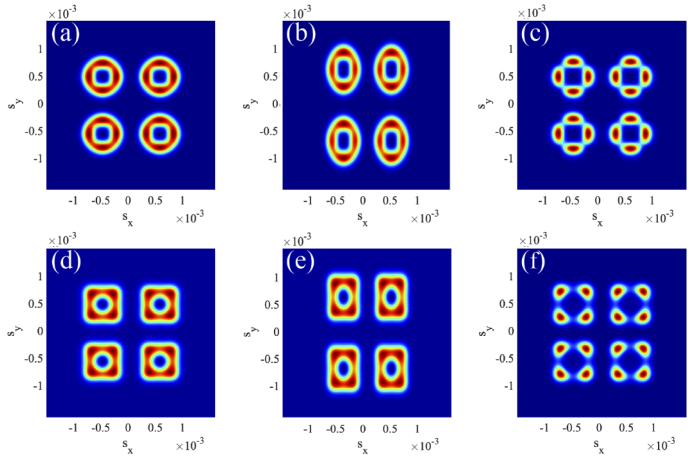

Fig. 7. Normalized spectral intensity distribution of the far field corresponding to Eq. (28): (a) $L_1 = 40$, $L_2 = 3$, $\delta_x = \delta_y = 1mm$; (b) $L_1 = 40$, $L_2 = 3$, $\delta_x = 1.2mm$, $\delta_y = 0.8mm$; (c) $L_1 = 40$, $L_2 = 8$, $\delta_x = \delta_y = 1mm$; (d) $L_2 = 25$, $L_1 = 2$, $\delta_x = \delta_y = 1mm$; (e) $L_2 = 25$, $L_1 = 2$, $\delta_x = 1.2mm$,$\delta_y = 0.8mm$; (f) $L_2 = 25$, $L_1 = 20$, $\delta_x = \delta_y = 1mm$.

Optics EXPRESS

where a and b are the weight coefficients.

As shown in the first row of Fig. 7, when setting $a = 1$, $b = -1$ and $L_1 > L_2$, the outer shape of lobes depends on μ_{c1}, the inner depends on μ_{r2}. The profile of a square hole inside a circle likes Chinese ancient copper coins. In turn, from the second row of Fig. 7, when setting $b = 1$, $a = -1$ and $L_2 > L_1$, the outer shape of lobes depends on μ_{r2}, the inner depends on μ_{c1}. The profile presents a circle hole inside a square. In addition, it can be clearly seen from Figs. 7(a) and 7(b) that each isotropic lobe changes into anisotropic one with choosing diffident effective correlation length along the x and y directions. Taking full note of Figs. 7(a) and 7(c), with the increase of the center hollow, each lobe of this combined array distribution is divided into four symmetrical and highlighted points. Similarly, Figs. 7(d)-(f) hold the same patterns.

5. Conclusion

In summary, we have designed random optical sources to generate novel type of far fields with hollow array distribution which consist of polar symmetric lobes and Cartesian symmetric lobes. It is shown that the array dimension, the distance of hollow lobes intensity profile, the size and shape of the inner and outer lobe contours and other features can be flexibly controlled by altering the source parameters. Finally, we have generalized the combination of the two degrees of coherence and account for two different far fields. The most important feature of the arrays in this article is that it remains structurally invariant on further propagation when the pattern is formed in the far field. The results of particular importance for certain applications in which a far field with controllable hollow lattice structure radiated by a random source must be sorely needed, such as material surface processing, optical particle manipulation, active imaging and communications.

Funding

National Natural Science Foundation of China (11874321); Fundamental Research Funds for the Central Universities (2018FZA3005).

Disclosures

The authors declare that there are no conflicts of interest related to this article.

References

1. L. Mandel and E. Wolf, in *Optical Coherence and Quantum Optics*, (Cambridge University, 1995).
2. F. Gori and M. Santarsiero, "Devising genuine spatial correlation functions," Opt. Lett. **32**(24), 3531–3533 (2007).
3. H. Lajunen and T. Saastamoinen, "Propagation characteristics of partially coherent beams with spatially varying correlations," Opt. Lett. **36**(20), 4104–4106 (2011).
4. Z. Mei and O. Korotkova, "Random sources generating ring-shaped beams," Opt. Lett. **38**(2), 91–93 (2013).
5. Z. Mei and O. Korotkova, "Cosine-Gaussian Schell-model sources," Opt. Lett. **38**(14), 2578–2580 (2013).
6. O. Korotkova, "Random sources for rectangular far fields," Opt. Lett. **39**(1), 64–67 (2014).
7. O. Korotkova and Z. Mei, "Convolution of degrees of coherence," Opt. Lett. **40**(13), 3073–3076 (2015).
8. L. Ma and S. A. Ponomarenko, "Free-space propagation of optical coherence lattices and periodicity reciprocity," Opt. Express **23**(2), 1848–1856 (2015).
9. C. Liang, X. Zhu, C. Mi, X. Peng, F. Wang, Y. Cai, and S. A. Ponomarenko, "High-quality partially coherent bessel beam array generation," Opt. Lett. **43**(13), 3188–3191 (2018).
10. L. Wan and D. Zhao, "Twisted Gaussian Schell-model array beams," Opt. Lett. **43**(15), 3554–3557 (2018).
11. Y. Zhou and D. Zhao, "Statistical properties of electromagnetic twisted Gaussian Schell-model array beams during propagation," Opt. Express **27**(14), 19624–19632 (2019).
12. V. Berger, O. Gauthier-Lafaye, and E. Costard, "Photonic band gaps and holography," J. Appl. Phys. **82**(1), 60–64 (1997).
13. M. Campbell, D. Sharp, M. Harrison, R. Denning, and A. Turberfield, "Fabrication of photonic crystals for the visible spectrum by holographic lithography," Nature **404**(6773), 53–56 (2000).
14. M. P. MacDonald, G. C. Spalding, and K. Dholakia, "Microfluidic sorting in an optical lattice," Adv. Phys. **426**(6965), 421–424 (2003).
15. I. Bloch, "Ultracold quantum gases in optical lattices," Nat. Phys. **1**(1), 23–30 (2005).

Optics EXPRESS

16. M. Lewenstein, A. Sanpera, V. Ahufinger, B. Damski, A. Sen, and U. Sen, "Ultracold atomic gases in optical lattices: mimicking condensed matter physics and beyond," Adv. Phys. **56**(2), 243–379 (2007).
17. L. Ma and S. A. Ponomarenko, "Optical coherence gratings and lattices," Opt. Lett. **39**(23), 6656–6659 (2014).
18. Z. Mei, D. Zhao, O. Korotkova, and Y. Mao, "Gaussian Schell-model arrays," Opt. Lett. **40**(23), 5662 (2015).
19. L. Wan and D. Zhao, "Optical coherence grids and their propagation characteristics," Opt. Express **26**(2), 2168–2178 (2018).
20. Z. Mei and O. Korotkova, "Sources for random arrays with structured complex degree of coherence," Opt. Lett. **43**(11), 2676–2679 (2018).
21. Y. Chen, S. A. Ponomarenko, and Y. Cai, "Experimental generation of optical coherence lattices," Appl. Phys. Lett. **109**(6), 061107 (2016).
22. C. Liang, C. Mi, F. Wang, Y. Cai, and S. A. Ponomarenko, "Vector optical coherence lattices generating controllable far-field beam profiles," Opt. Express **25**(9), 9872–9885 (2017).
23. Z. Liu and D. Zhao, "Experimental generation of a kind of reversal rotating beams," Opt. Express **28**(3), 2884–2894 (2020).
24. T. Kuga, Y. Torii, N. Shiokawa, T. Hirano, Y. Shimizu, and H. Sasada, "Novel optical trap of atoms with a doughnut beam," Phys. Rev. Lett. **78**(25), 4713–4716 (1997).
25. M. Yan, J. Yin, and Y. Zhu, "Dark-hollow-beam guiding and splitting of a low-velocity atomic beam," J. Opt. Soc. Am. B **17**(11), 1817–1820 (2000).
26. H. Izadpanah, T. Elbatt, V. Kukshya, F. Dolezal, and B. K. Ryu, "Atomic trapping and guiding by quasi-dark hollow beams," IEEE Wireless Commun. **10**(2), 45–53 (2003).
27. Z. Wang, Y. Dong, and Q. Lin, "Atomic trapping and guiding by quasi-dark hollow beams," J. Opt. A: Pure Appl. Opt. **7**(3), 147–153 (2005).
28. Y. Cai, X. Lu, and Q. Lin, "Hollow Gaussian beams and their propagation properties," Opt. Lett. **28**(13), 1084–1086 (2003).
29. Y. Cai, C. Chen, and F. Wang, "Modified hollow Gaussian beam and its paraxial propagation," Opt. Commun. **278**(1), 34–41 (2007).
30. Z. Mei and D. Zhao, "Controllable elliptical dark-hollow beams," J. Opt. Soc. Am. A **23**(4), 919–925 (2006).
31. V. V. Kotlyar, R. V. Skidanov, S. N. Khonina, and V. A. Soifer, "Hypergeometric modes," Opt. Lett. **32**(7), 742–744 (2007).
32. E. Karimi, G. Zito, B. Piccirillo, L. Marrucci, and E. Santamato, "Hypergeometric-Gaussian modes," Opt. Lett. **32**(21), 3053–3055 (2007).
33. Q. Sun, K. Zhou, G. Fang, G. Zhang, Z. Liu, and S. Liu, "Hollow sinh-Gaussian beams and their paraxial properties," Opt. Express **20**(9), 9682–9691 (2012).
34. B. Tang, S. Jiang, C. Jiang, and H. Zhu, "Propagation properties of hollow sinh-Gaussian beams through fractional Fourier transform optical systems," Opt. Laser Technol. **59**, 116–122 (2014).
35. D. Zou, X. Li, X. Pang, H. Zheng, and Y. Ge, "Propagation properties of hollow sinh-Gaussian beams in quadratic-index medium," Opt. Commun. **401**, 54–58 (2017).
36. S. Vyas, Y. Kozawa, and S. Sato, "Generation of radially polarized Bessel-Gaussian beams from c-cut Nd:YVO4 laser," Opt. Lett. **39**(4), 1101–1104 (2014).
37. Y. Chen, L. Liu, F. Wang, C. Zhao, and Y. Cai, "Elliptical Laguerre-Gaussian correlated Schell-model beam," Opt. Express **22**(11), 13975–13987 (2014).
38. Y. Xia and J. P. Yin, "Generation of a focused hollow beam by an 2pi-phase plate and its application in atom or molecule optics," J. Opt. Soc. Am. A **22**(3), 529–536 (2005).
39. S. Marksteiner, C. M. Savage, P. Zoller, and S. L. Rolston, "Coherent atomic waveguides from hollow optical fibers: quantized atomic motion," Phys. Rev. A **50**(3), 2680–2690 (1994).
40. Z. Liu, H. Zhao, J. Liu, J. Lin, M. A. Ahmad, and S. Liu, "Generation of hollow Gaussian beams by spatial filtering," Opt. Lett. **32**(15), 2076–2078 (2007).
41. H. S. Lee, B. W. Atewart, K. Choi, and H. Fenichel, "Holographic non-diverging hollow beam," Phys. Rev. A **49**(6), 4922–4927 (1994).